A thermodynamic quest for topological metal transition

L.J. Ding* and Y. Zhong

Department of Physics and Electronic-Information Engineering, Hubei Engineering University, Xiaogan, Hubei, 432000, China

*Corresponding author: dinglinjie82@126.com

We study the topological quantum phase transition (TQPT) between a normal insulator and a topological metal state in the three-leg diamond lattices via thermodynamic means. Doing a unitary transformation, the Hilbert space of the system is divided into two independent subspaces: trivial h_1 and topologically nontrivial h_2 such that the TQPT is regarded as an ordinary insulator-metal transition plus a topological insulator transition. The thermal Drude weight portrays well the insulator (D_{th}=0) and metal (D_{th}>0) ground states with the low-temperature gapped and gapless low-lying excitations featured as $D_{th} \propto e^{-\Delta_g/k_BT}$ and $D_{th}-T$ linear relation, respectively. The ordinary insulator-metal transition is manifested not only by the quantum critical scaling of thermal Drude weight, but also by the critical divergence of Grüneisen ratio (GR~-T^{-1}) with an asymmetric scaling universal curve. Differently, the topological insulator transition occurs in h_2 subspace protected by a hidden inversion symmetry, which is demonstrated by the switching of winding number with band inversion as well as the finite GR nearby 1/2 with a symmetric scaling universal curve, implying the proximate self-duality of quantum critical point. Our findings provide a novel thermodynamic perspective on topological metal transition.

1 Introduction

It has attracted extentive interest to identify, classify and engineer the novel topological quantum states based on the topological symmetry and band theory [1-4]. The topological

insulator (TI) [1,5], topological semimetal (TSM) [6,7] and topological metal (TM) [8-13] are prototype examples of topological phases. TI has a fully gapped bulk band structure with symmetry-protected edge states falling inside the gap, which can be characterized by the corresponding topological invariant such as Chern (Z_2) number, winding number, Zak phase and so on [1,2,14,15]. TSM is signaled by the band touching point or node at the Fermi level, at which the energy gap is closed and the energy bands are degenerate at a particular momentum in the first Brillouin zone [6]. The representive examples are the Weyl and Dirac semimetals, which showcase linear relation around the Weyl and Dirac points with double and fourfold degeneracy, respectively. Differently, TM bridges the ordinary metal state and TI state, manifesting the nontrivial edge states within the gapless bulk states [10].

Usually, topological quantum phase transition (TQPT) takes place at zero temperature with bulk band gap closing and TSM as the topological quantum criticality. Meanwhile, it is accompanied by the topological invariant switched off with band inversion [16,17]. However, the TQPT into TM is different from the semimetal. It has been designed and realized in 2D particle-hole or time-reversal symmetric system with or without adjusting the magnetic flux [8,9]. Furthermore, the intrinsic TMs have been demonstrated in 2D T-graphene and quasi-1D trivial spinless models like dimerized two-leg ladders and three-leg diamond lattices, in which the topologically-protected nontrivial edge states hidden within the gapless bulk states [10-13]. Strikingly, in the three-leg diamond lattices, the Hilbert space of the system could be divided into two independent subspaces after performing a unitary transformation. One is a trivial subspace, and the other is a toplogically nontrivial one. Upon tuning the hopping parameters, it yields a TQPT from normal insulator (NI) to inversion symmetry-protected TM phase. In experiment,

there is no access to detect the TM phase transition occurrs at zero temperature, some new thermodynamic means should be explored at finite temperatures to manifest the TQPTs, since the quantum criticality has a huge effect on the finite temperature thermodynamics [18,19]. How to feature the low-lying excitations of NI and TM phases? How to characterize the TM phase transition and demonstrate the self-duality of quantum critical point (QCP) by thermodynamic means?

Here, we focus on the three-leg diamond lattices to adress these questions. It is constructed by way of trivial spinless quantum wire arrays with each unit cell containing three sublattices (Fig. 1(a)), which is described by a tight-banding model without explicit symmetry. Doing a unitary transformation, the Hilbert space of the system is segmented into two independent subspaces: a trivial h_1 and a topologically nontrivial h_2 [12,13]. For comparison, first, turning off some intracell and intercell hoppings, one can obtain a diamond chain with a flat band lying in the Fermi level in h_1 subspace but a TI transition in h_2 subspace. In h_2 subspace, the exact self-duality of QCP is demonstrated by the constant of Grüneisen ratio (GR=1/2). After recovering and tuning the corresponding intracell and intercell hoppings, a TQPT between a normal insulator (NI) and TM is gained. In such phase transition, one energy band passes the Fermi level, while the gap between the other two bands is closed and reopened, taking on the zero-energy edge states within the gapless bulk states. The gapped NI and gapless TM phases are signaled by the thermal Drude weight with $D_{th} \propto e^{-\Delta_g/k_BT}$ and T-linear relation at low temperatures, respectively. Meanwhile, in h_2 subspace, the switching of winding number and divergence of correlation length signal the TQPT clearly. The proximate self-duality of QCP is manifested by the finite GR nearby 1/2. Furthermore, the scaled GR falls on a universal curve with asymmetrical and symmetrical

structures in the whole Hilbert space and h_2 subspace, respectively, implying the intrinsic TM transition.

2 Model Hamiltonian and method

We consider the three-leg diamond lattices as sketched in Fig. 1(a), which is governed by the tight-banding Hamiltonian [12,13]

$$H=\sum_{l=1}^{L}\left\{t_0 a_l^{\dagger}b_l+t_1(a_l^{\dagger}c_l+b_l^{\dagger}c_l)+t_2(c_l^{\dagger}a_{l+1}+c_l^{\dagger}b_{l+1})+t_3(a_l^{\dagger}a_{l+1}+b_l^{\dagger}b_{l+1})+H.c.\right\}, \qquad (1)$$

where L is the number of unit cell. $y_l\left(y_l^{\dagger}\right)$ annihilates (creates) a spinless electron on sublattice $y\in(a,b,c)$ of the lth unit cell. t_0 and t_1 are the intracell hopping, while t_2 and t_3 are the intercell hopping. Here, t_1=1 is selected as an energy unit. In the momentum space, it leads to $H=\sum_k \Psi_k^{\dagger}H(k)\Psi_k$ with $\Psi_k^{\dagger}=\left(a_k^{+},b_k^{+},c_k^{+}\right)$ and

$$H(k)=\begin{bmatrix} 2t_3\cos k & t_0 & t_1+t_2e^{-ik} \\ t_0 & 2t_3\cos k & t_1+t_2e^{-ik} \\ t_1+t_2e^{ik} & t_1+t_2e^{ik} & 0 \end{bmatrix}. \qquad (2)$$

If a unitary transformation is employed, the Hamiltonian will be block-diagonalized as,

$$H_D(k)=U^{-1}H(k)U=\begin{bmatrix} h_1(k) & 0 \\ 0 & h_2(k) \end{bmatrix}, \qquad (3)$$

with the unitary matrix

$$U=\frac{1}{\sqrt{2}}\begin{bmatrix} -1 & 1 & 0 \\ 1 & 1 & 0 \\ 0 & 0 & \sqrt{2} \end{bmatrix}. \qquad (4)$$

Thus, the Hilbert space becomes two separable subspaces such that one can obtain two independent blocks $h_1(k)=2t_3\cos k-t_0$ and

$$h_2(k)=\begin{bmatrix} 2t_3\cos k+t_0 & \sqrt{2}\left(t_1+t_2e^{-ik}\right) \\ \sqrt{2}\left(t_1+t_2e^{ik}\right) & 0 \end{bmatrix}=d_0\sigma_0+\vec{d}\cdot\vec{\sigma}. \qquad (5)$$

Herein, $d_0=\left(2t_3\cos k+t_0\right)/2$ and σ_0 is the 2×2 identical matrix. $\vec{\sigma}=\left(\sigma_x,\sigma_y,\sigma_z\right)$ are the Pauli matrices and the effective magnetic field (i.e., the Anderson pseudospin vector) $\vec{d}=\left(d_x,d_y,d_z\right)=\left(\sqrt{2}\left(t_1+t_2\cos k\right),\sqrt{2}t_2\sin k,d_0\right)$. Accordingly, one can get the energies of the Bloch bands,

$$E_1=2t_3\cos k-t_0,\ \ E_{\pm}=d_0\pm\sqrt{d_x^2+d_y^2+d_z^2}\ . \tag{6}$$

The thermodynamic quantities such as free-energy density, entropy and specific heat are expressed as [19],

$$F=-\frac{1}{\beta}\sum_{p=1,\pm}\int_{-\pi}^{\pi}\frac{dk}{2\pi}\ln\left(1+e^{-\beta E_p(k)}\right), \tag{7}$$

$$S=-\left(\partial F/\partial T\right)=k_B\cdot\left\{\sum_{p=1,\pm}\int_{-\pi}^{\pi}\frac{dk}{2\pi}\ln\left(1+e^{-\beta E_p(k)}\right)+\beta\sum_{p=1,\pm}\int_{-\pi}^{\pi}\frac{dk}{2\pi}E_p(k)\,f\left(E_p(k)\right)\right\}, \tag{8}$$

$$C_V=T\left(\partial S/\partial T\right)=k_B\cdot\left\{\beta^2\sum_{p=1,\pm}\int_{-\pi}^{\pi}\frac{dk}{2\pi}E_p^2(k)\cdot e^{\beta E_p(k)}\cdot f^2\left(E_p(k)\right)\right\}, \tag{9}$$

with $\beta=1/k_BT$ and the Fermi-Dirac distribution function $f\left(E_p(k)\right)=\dfrac{1}{1+e^{\beta E_p(k)}}$.

In an adiabatic process, the GR is attained as [20-22]

$$\Gamma\left(T,t_2\right)=\frac{1}{T}\left(\frac{dT}{dt_2}\right)_S=-\frac{\left(\partial S/\partial t_2\right)_T}{T\left(\partial S/\partial T\right)_{t_2}}=-\frac{\left(\partial S/\partial t_2\right)_T}{C_V}. \tag{10}$$

3 Results and discussion

For simplity, we first consider t_0=t_3=0 case and set t_1=1 as an energy unit. At this time, the system is reduced into a diamond chain with only the nearest neighbor hoppings, which is, indeed, a bipartite lattice with two different connective sites [23,24]. The rim sites have two nearst neighbor sites while the hub sites own four ones. From the subspace h_1, one can obtain a flat band pinned to the Fermi level, the quenched kinetic energy of which causes localization and zero wave group velocity, regarded as irreducible compact localized state [23], as shown in Fig. 1(b1)-(b3).

In subspace $h_2 = d_x\sigma_x + d_y\sigma_y$, it hosts the time reversal (TR), particle-hole (PH) and chiral (C) symmetries [2],

$$h_2^*(-k) = h_2(k),\ \ \sigma_z h_2^*(-k)\sigma_z = -h_2(k),\ \ \sigma_z h_2(k)\sigma_z = -h_2(k), \tag{11}$$

belonging to the BDI symmetry class. The subsystem h_2 also displays the inversion symmetry $\sigma_x h_2(k)\sigma_x = h_2(-k)$ [13], similar to the SSH model, and takes on interesting topological bands, which can be characterized and labelled by the topological invariant-Zak phase [14,15],

$$\varphi_{Zak} = \oint_{BZ} A(k)dk\ . \tag{12}$$

The Berry connection is $A(k) = i\langle u_k|\partial_k|u_k\rangle$ with $|u_k\rangle$ the normalized eigenvector for $E_{\pm}$, which is divergent at the band gap closing, reflecting the TQPT. Within the bulk-edge correspondence, the gap closing and reopening give rise to the switching of edge states, which is similar to the band inversion. It is identified by the symmetry of wavefunction parity defined as even symmetry with $|u_k+\rangle = \begin{pmatrix}1\\1\end{pmatrix}$ and odd symmetry with $|u_k-\rangle = \begin{pmatrix}-1\\1\end{pmatrix}$ [16,17]. The phase transition from topologically trivial ($\varphi_{Zak} = 0$) to nontrivial ($\varphi_{Zak} = \pi$) one is illustrated in Fig. 1(b1)-(b3) with band inversion at $k = \pi$, at which it shows Dirac-like bands at t_2=t_{2c}=1.0 with the energy gap closed (Fig. 1(b2)). Even if the intracell nearst neighbor hopping t_0 between top and bottom sites is turned on, it still does not give dispersion to the flat band but pull it down into the Fermi sea [25], destroying the topology in subspace h_2 (Fig. 1(b4)).

Besides, the profile of Berry connection in momentum space is plotted in Fig. 1(c1) for different t_2 values around t_{2c}=1.0 [26,27]. There is a negative dip around $k = \pi$, which grows as t_2 increases and becomes sharper and sharper approaching the QCP t_{2c}=1.0. Beyond t_{2c}, the Berry connection takes on a positive peak at $k = \pi$, which is suppressed with t_2 further ascending. It is evidenced that there is a TQPT at t_{2c}=1.0. Besides, as the wave vector traverses across the entire

first Brillouin zone, it gives rise to the winding of Bloch vector around the origin with the chiral winding number $N_w = \varphi_{Zak}/\pi$. The TQPT is clearly portrayed in Fig. 1(c2), wherein the winding number jumps from 0 to 1 at t_{2c}=1.0, with 1 being the topological invariant difference.

Furthermore, the GR related to the magnetocaloric-like effect, is a good thermodynamic quantity to diagnose the TQPT and characterize its self-duality [20,22]. In subspace h_2, Fig. 1(d1) presents the GR as a function of t_2 in the temperature interval of [0.01,0.05], which displays a symmetric valley-peak structure with respect to t_{2c}. Meanwhile, it shows an asymptotic quantum critical scaling form $\Gamma^{h_2}\left(T,t_{2c}\right)=\frac{1}{t_2-t_{2c}}\Phi\left(\frac{t_2-t_{2c}}{k_BT}\right)$ with $\Phi(x)$ the scaling function [19, 22]. As $T\to 0$, a critical divergency $\Gamma^{h_2}\left(T,t_{2c}\right)\sim 1/\left(t_2-t_{2c}\right)$ is taken on with universal prefactors $\Phi(x\to\pm\infty)$=1, which is distinguished with the Luttinger liquid QPT in Heisenberg chain [28]. Evidently, by performing the inversion and translational symmetry transformation: $\hat{P}a_l\hat{P}^{-1}=b_l$, $\hat{P}b_l\hat{P}^{-1}=a_l$ and $\hat{T}a_l\hat{T}^{-1}=a_{l+1}$, $\hat{T}b_l\hat{T}^{-1}=b_{l+1}$ [29], the Hamiltonian posseses the same form via the parameter exchange as $t_1\leftrightarrow t_2$. Thus, one can decouple the h_2 subsystem as $h_2\left(t_2\right)=H_1+t_2H_2$. Doing the unitary or antiunitary transformation, $UH_1U^{-1}=H_2$, $UH_2U^{-1}=H_1$, it manifests an Abelian Z_2 symmetry $Uh_2\left(t_{2c}\right)U^{-1}=h_2\left(t_{2c}\right)$ at the QCP with self-duality, around which, two gapped phases can be mapped into each other [19,20]. At the QCP, the self-duality leads to that $\left\langle H_1\right\rangle_T=\left\langle UH_1U^{-1}\right\rangle_T=\left\langle H_2\right\rangle_T=\frac{1}{2}\left\langle h_2\left(t_{2c}\right)\right\rangle_T$. Accordingly, the GR in h_2 subspace at the QCP reads as,

$$\Gamma^{h_2}\left(T,t_{2c}\right)=\frac{\partial\left\langle H_2\right\rangle_T/\partial T}{\partial\left\langle h_2\left(t_{2c}\right)\right\rangle_T/\partial T}=\frac{1}{2}, \tag{13}$$

which is irrespective of temperature, as shown in Fig. 1(d2).

Strikingly, if the next nearest neighbor hopping (t_3) between adjacent unit cells is turned on, the

flat band will be dispersive. From subspace h_2, it is found that if $t_3 \neq t_2/2$ and $t_0 \neq t_1 = 1.0$ the subsystem only posseses trivial phases without any topology, as a result of the destruction of PH, C and inversion symmetries [12]. Hereafter, we set $t_3 = t_2/2$ and $t_0 = t_1 = 1.0$. As such, the TR symmetry $h_2^*(-k) = h_2(k)$ still persists, but the PH and C symmetries are broken, which is belonging to the AI class [2]. Meanwhile, the hidden inversion symmetry of subspace h_2 is revived $Ph_2(k)P^{-1} = h_2(-k)$ with inversion operator $P = \frac{1}{3}\begin{pmatrix} 1 & 2\sqrt{2} \\ 2\sqrt{2} & -1 \end{pmatrix}$.

In Fig. 2(a), below $t_{2c} = 1.0$, the band E_1 resides in the Fermi sea, while the bands $E_\pm$ present topologically trivial property, implying the normal insulator. With increasing t_2, one can find that from Fig. 2(b), the gap closes, yielding a TQPT for bands $E_\pm$ with linear relation around $k_c = \pi$, i.e., $E_\pm \propto |k - k_c|^z$ with $z = 1$. Meanwhile, the band E_1 is pushed up and touches the Fermi level with a quatratic relation around $k_c = 0$, resulting in the dynamic critical exponent $z = 2$. After the TQPT, the bands $E_\pm$ shows topologically nontrivial along with band inversion at $k = \pi$ and gap reopened, as plotted in Fig. 2(c). Nevertheless, the band E_1 crosses the Fermi level and manifests a metallic state. Thus, the whole system is a conductor in a topologically nontrivial phase, which is regarded as a toplogical metal.

In subspace h_2, we further present the profile of Berry connection in momentum space in Fig. 2(d), which shows a sharp peak or dip at two sides of t_{2c} with opposite sign. The divergence of Berry connection gives rise to the critical behavior $A(k_0 = \pi, t_2) \propto |t_2 - t_{2c}|^{-\gamma}$ with the critical exponent $\gamma = 1$ (the inset in Fig. 2(d)). Besides, in Fig. 2(e), the winding number manifests the TQPT evidently, which jumps from 0 to 1 at $t_{2c} = 1.0$ with 1 being the topological invariant difference. In order to quantitatively describe the topological criticality, a correlation length ξ_k in the momentum space is defined by the inverse of the full width at half maximum of Berry

connection [26], as shown in the left inset in Fig. 2(f). Fig. 2(f) presents the correlation length ξ_k versus t_2, which diverges as t_2 approaches the critical value t_{2c}=1.0. Its double logarithm is plotted in the right inset of Fig. 2(f), in which the critical scaling behavior manifests $\xi_k \propto \left|t_2 - t_{2c}\right|^{-\nu}$ with ν=1.

In addition, the quantum criticality has a huge effect on the thermodynamics at finite temperatures [18,19,22], giving experimental access to its observation. The thermal Drude weight that is defined as $D_{th} = \frac{\pi\beta^2}{ZN} \sum_{\substack{n,m \\ E_n=E_m}} e^{-\beta E_n} \left|\left\langle n \left| j_{th} \right| m \right\rangle\right|^2$ with j_{th} the energy current and Z the partition function [30], is employed to feature the gapless (D_{th}>0) and gapped (D_{th}=0) phases. In subspace h_1, the thermal Drude weight increases from zero to a finite value continuously (Fig. 3(a)), indicating an insulator-metal transition, analogous to the Luttinger liquid QPT. Around the QCP, it presents a QC scaling $D_{th}^{h_1} \propto \left(t_2 - t_{2c}\right)^{1/\delta}$ with δ=1.867 (the inset in Fig. 3(a)). At finite temperatures, it presents a critical scaling $D_{th}^{h_1}/T \propto T^{\beta}$ in Fig. 3(b). Its double-logarithm reflects the critical exponent β=0.489. Besides, in the inset of Fig. 3(b), the specific heat displays $C_V^{h_1}/T \propto T^{-\alpha}$ critical divergence with α=0.488 at the QCP, denoting a proximate $T^{1/2}$ critical behavior. In another way, one can obtain the critical exponent α=1/2 from the scaling relation α=2-(d+z)/z with d=1 and z=2 [19,31], demonstrating the $T^{1/2}$ critical behavior of specific heat. Thus, one can obtain $\alpha+\beta(1+\delta)$=1.890 for the obtained quantum critical exponents (δ,α,β)=(1.867,0.488,0.489), in accordance with the Essam-Fisher law $\alpha+\beta(1+\delta)$=2 [32].

In Fig. 3(a), one can find that in subspace h_2, the thermal Drude weight presents a sharp peak at the QCP, implying the gapless quantum criticality regarded as a topological semimetal (Fig. 2(b)). Otherwise, it stays at zero value, suggesting the gapped topological insulators [19]. This gapless quantum criticality is further manifested by the T-linear relation of $D_{th}^{h_2}$ in Fig. 3(b), where

$D_{th}^{h_2}/T$ keeps a constant independent of temperature.

At finite temperatures, the gapped low-lying excitation is demonstrated for $t_2<t_{2c}$ by the temperature dependence of thermal Drude weight in two subspaces in Fig. 3(c), which is exponetially activated: $D_{th} \propto e^{-\Delta_g/k_BT}$. The slope of the curve lnD_{th} versus $1/T$ in the inset reflects the energy gap $\Delta_g \propto \left|t_2 - t_{2c}\right|^{z\nu}$ with $z\nu$=1. Thus, one can obtain ν=1/2 and 1 with z=2 and 1 in subspaces h_1 and h_2, respectively, consistent with the critical scaling behavior of correlation length. Beyond t_{2c}, it is still exponentially activated in subspace h_2, as shown in Fig. 3(a) and the left inset. However, in subspace h_1, the thermal Drude weight displays zero energy gap (left inset) and presents a T-linear relation as $T\rightarrow 0$ (right inset), demonstrating gapless metallic state.

From the above analysis of thermal Drude weight, one can get the gapped insulator transition into gapless metal in subspace h_1, and one gapped insulator transition into another gapped insulator in subspace h_2, but not feature the topological metal at finite temperatures. Here, we employ the GR to identify the topological quantum criticality. Although the whole system composes of subsystems h_1 and h_2, the subpace h_1 determines the insulator-metal transition. In Fig. 4(a), the GR presents a zero-crossing point with sign changed, which manifests an asymptotic QC scaling form $\Gamma\left(T,t_{2c}\right)=\dfrac{1}{t_2-t_{2c}}\Re\left(\dfrac{t_2-t_{2c}}{k_BT}\right)$ with $\Re\left(y\right)$ the scaling function [19]. Upon cooling down to zero temperature, the asymptotics $y=(t_2-t_{2c})/k_BT\rightarrow\pm\infty$ generate characteristic zero-temperature divergency $\Gamma(T,t_{2c})\sim 1/(t_2-t_{2c})$ with universal prefactors $\Phi(y\rightarrow\pm\infty)$=1 and 1/2, respectively, which is akin to the Luttinger liquid QPT in Heisenberg chain [28]. At this time, the self-duality is broken, because the gapless and gapped spectra in the two phases cannot be mapped into each other [19,20]. At low temperatures, the GR presents a power-law divergence: $\Gamma(T,t_{2c})$

$\sim$-T^{-1} at the QCP in Fig. 4(b), implying the conventional QPT without self-duality [33], which is further confirmed by the scaling transformation $\Gamma(T,t_2)\times(t_2-t_{2c})$ in Fig. 4(c) that perfectly fall on a universal asymmetrical curve. However, in subspace h_2, its topological property is demonstrated by the valley-peak symmetric structure of GR in Fig. 4(d) around t_{2c}, at which the asymptotics $x=(t_2-t_{2c})/k_BT \to \pm\infty$ generate a zero-temperature divergency $\Gamma^{h_2}\left(T,t_{2c}\right)\sim 1/\left(t_2-t_{2c}\right)$ with universal prefactors $\Phi(x\to\pm\infty)=1$. The diagonal element $2t_3\cos k+t_0$ in h_2 is seen as a perturbation such that the expanded GR $\Gamma\left(T,t_{2c}\right)=\Gamma\left(0,t_{2c}\right)+\sum_n \frac{\Gamma^{(n)}\left(0,t_{2c}\right)}{n!}T^n$ [20] is finite but still approaches 1/2 (Fig. 4(e)), demonstrating the proximate self-duality of the QCP. Meanwhile, the scaling transformation $\Gamma^{h_2}\left(T,t_{2c}\right)\times\left(t_2-t_{2c}\right)$ perfectly falls on a universal symmetric curve with respective to t_{2c}=1.0. Therefore, the GR serves as a superb tool to diagnose the topological quantum criticality and topological metal.

4. Conclusion

In conclusion, the TQPT between a NI and a TM state in the three-leg diamond lattices, the Hilbert space of which is segmented into a trivial subspace h_1 and a topological nontrivial one h_2 with a unitary transformation, is investigated by thermodynamic means. Turning off some intracell and intercell hoppings, in addition to a trivial flat band, it manifests a TI transition with the QCP being exactly self-dual, which is demonstrated by the constant of GR=1/2 irrespective of temperature in h_2 subspace. After recovering and tuning the corresponding hoppings, the trivial flat band becomes dispersive, resulting in a TM transition, which is regarded as an ordinary insulator-metal transition together with a TI transition. Upon cooling down to zero temperature, the thermal Drude weight portrays well the gapped insulator (D_{th}=0) and gapless metal (D_{th}>0) phases, which are further featured by $D_{th}\propto e^{-\Delta_g/k_BT}$ and T-linear relation at low temperatures,

respectively. The ordinary insulator-metal transition is captured by the quantum critical scaling of thermal Drude weight and specific heat, whose exponents fulfill the Essam-Fisher law, similar to the general Luttinger liquid QPT. Meanwhile, the GR presents a zero-crossing and sign change with a critical divergence ($\sim$-T^{-1}) and an asymmetric scaling universal curve at low temperatures. However, the TI transition takes place in h_2 subspace protected by a hidden inversion symmetry, which is demonstrated not only by the switching of winding number, divergence of correlation length and band inversion, but also by the sharp peak of thermal Drude weight as well as the finite GR nearby 1/2 with a symmetric scaling universal curve, implying the proximate self-duality of QCP. Our findings manifest a novel thermodynamic perspective on TM transition.

Acknowledgements

This work is supported by Chongqing National Science Fundation (cstc2021jcyj-msxmX0878, CSTB2022BSXM-JCX0102), China.

References

[1] X. L. Qi, and S. C. Zhang, Topological insulators and superconductors. Rev. Mod. Phys. 83, 1057 (2011).

[2] C. K. Chiu, J. C. Y. Teo, A. P. Schnyder, and S. Ryu, Classification of topological quantum matter with symmetries. Rev. Mod. Phys. 88, 035005 (2016).

[3] A. Bansil, Hsin Lin, and Tanmoy Das, Colloquium: Topological band theory, Rev. Mod. Phys. 88, 021004 (2016).

[4] O. Gröning, S. Y. Wang, X. L.Yao, C. A. Pignedoli, G. B. Barin, C. Daniels, A. Cupo, V. Meunier, X. L. Feng, A. Narita, K. Müllen, P. Ruffieux, and R. Fasel, Engineering of robust topological quantum phases in graphene nanoribbons. Nature 560, 209 (2018).

[5] H. M. Guo, A brief review on one-dimensional topological insulators and Superconductors, Sci. China-Phys. Mech. Astron. 59, 637401 (2016).

[6] A. A. Burkov, Topological semimetals, Nat. Mater. 15, 1145 (2016).

[7] A. Bernevig, H. M. Weng, Z. Fang, and X. Dai, Recent Progress in the Study of Topological Semimetals, J. Phys. Soc. Jpn. 87, 041001 (2018).

[8] X. Z. Ying, and A. Kamenev, Symmetry-Protected Topological Metals, Phys. Rev. Lett. **121**, 086810 (2018).

[9] L. C. Xie, H. C. Wu , L. Jin, and Z. Song, Time-reversal symmetric topological metal, Phys. Rev. B 104, 165422 (2021).

[10] L. Yan, D. Zhang, X. J. Wang, and J.Y. Yan, Intrinsic topological metal state in T-graphene, New J. Phys. 25, 043020 (2023).

[11] M. Jangjan, and M. V. Hosseini, Floquet engineering of topological metal states and hybridization of edge states with bulk states in dimerized two- leg ladders, Sci. Rep. 10, 14256 (2020).

[12] M. Jangjan, and M. V. Hosseini, Topological phase transition between a normal insulator and a topological metal state in a quasi- one- dimensional system, Sci. Rep. 11, 12966 (2021).

[13] Z. W. Zuo, L. X. Lv, and D. W. Kang, Topological metals constructed by sliding quantum wire arrays, Phys. Rev. B 107, 195142 (2023).

[14] J. Zak, Berry's Phase for Energy Bands in Solids. Phys. Rev. Lett. 62, 2747 (1989).

[15] M. Atala, M. Aidelsburger, J. T. Barreiro, D. Abanin, T. Kitagawa, E. Demler, and I. Bloch, Direct measurement of the Zak phase in topological Bloch bands. Nat. Phys. 9, 795 (2013).

[16] L. J. Ding, and Y. Zhong, Half-valley semimetal and largest inverse topological caloric effect at topological quantum criticality in the chiralsymmetric AIII class, Appl. Phys. Lett. 123, 243104 (2023).

[17] S. Cheon, T. H. Kim, S. H. Lee, and H. W. Yeom, Chiral solitons in a coupled double Peierls chain. Science **350**, 182 (2015).

[18] I. Frérot, and T. Roscilde, Reconstructing the quantum critical fan of strongly correlated systems using quantum correlations, Nat. Commun., 10, 577 (2019).

[19] L. J. Ding, Y. X. Xiang, and Y. Zhong, Unusual thermodynamic signature of topological quantum criticality in two coupled Su-Schrieffer-Heeger chains, Results Phys. 42, 106018 (2022).

[20] L. Zhang, Universal Thermodynamic Signature of Self-Dual Quantum Critical Points, Phys. Rev. Lett. 123, 230601 (2019).

[21] Q. Luo, Analytical results for the unusual Grüneisen ratio in the quantum Ising model with Dzyaloshinskii-Moriya interaction, Phys. Rev. B 105, L060401 (2022).

[22] L. J. Ding, Y. L. Sun, and Y. Zhong, Characterization of gapless topological quantum phase transition via magnetocaloric effect, Results Phys. 59, 107572 (2024).

[23] R. Khomeriki and S. Flach, Landau-Zener Bloch Oscillations with Perturbed Flat Bands, Phys. Rev. Lett. 116, 245301 (2016).

[24] M. N. Huda, S. Kezilebieke, and P. Liljeroth, Designer flat bands in quasi-one-dimensional atomic lattices, Phys. Rev. Research 2, 043426 (2020).

[25] L. Morales-Inostroza and R. A. Vicencio, Simple method to construct flat-band lattices, Phys. Rev. A 94, 043831 (2016).

[26] Z. J. Sun, M. H. Deng, and F. X. Li, Kibble-Zurek behavior in one-dimensional disordered topological insulators, Phys. Rev. B 106, 134203 (2022).

[27] R. R. Kumar, N. Roy, Y. R. Kartik, S. Rahul, S. Sarkar, Signatures of topological phase transition on a quantum critical line, Phys. Rev. B 107, 205114 (2023).

[28] O. Breunig, M. Garst, A. Klümper, J. Rohrkamp, M.M. Turnbull, T. Lorenz, Quantum criticality in the spin-1/2 Heisenberg chain system copper pyrazine dinitrate, Sci. Adv. 3, eaao3773 (2017).

[29] C. Li, S. Lin, G. Zhang, and Z. Song, Topological nodal points in two coupled Su-Schrieffer-Heeger chains. Phys. Rev. B 96, 125418 (2017).

[30] E. Orignac, R. Chitra, R. Citro, Thermal transport in one-dimensional spin gap systems, Phys. Rev. B 67, 134426 (2003).

[31] Y. Kono, T. Sakakibara, C. P. Aoyama, C. Hotta, M. M. Turnbull, C. P. Landee, Y. Takano, Field-Induced Quantum Criticality and Universal Temperature Dependence of the Magnetization of a Spin-1/2 Heisenberg Chain, Phys. Rev. Lett. 114, 037202 (2015).

[32] J.W. Essam, M.E. Fisher, Pade Approximant Studies of the Lattice Gas and Ising Ferromagnet below the Critical Point, J. Chem. Phys. 38, 802 (1963).

[33] H. Ryll, K. Kiefer, Ch. Rüegg, S. Ward, K.W. Krämer, D. Biner, P. Bouillot, E. Coira,T. Giamarchi, C. Kollath, Magnetic entropy landscape and Grüneisen parameter of a quantum spin ladder, Phys. Rev. B 89, 144416 (2014).

Figures and figure captions:

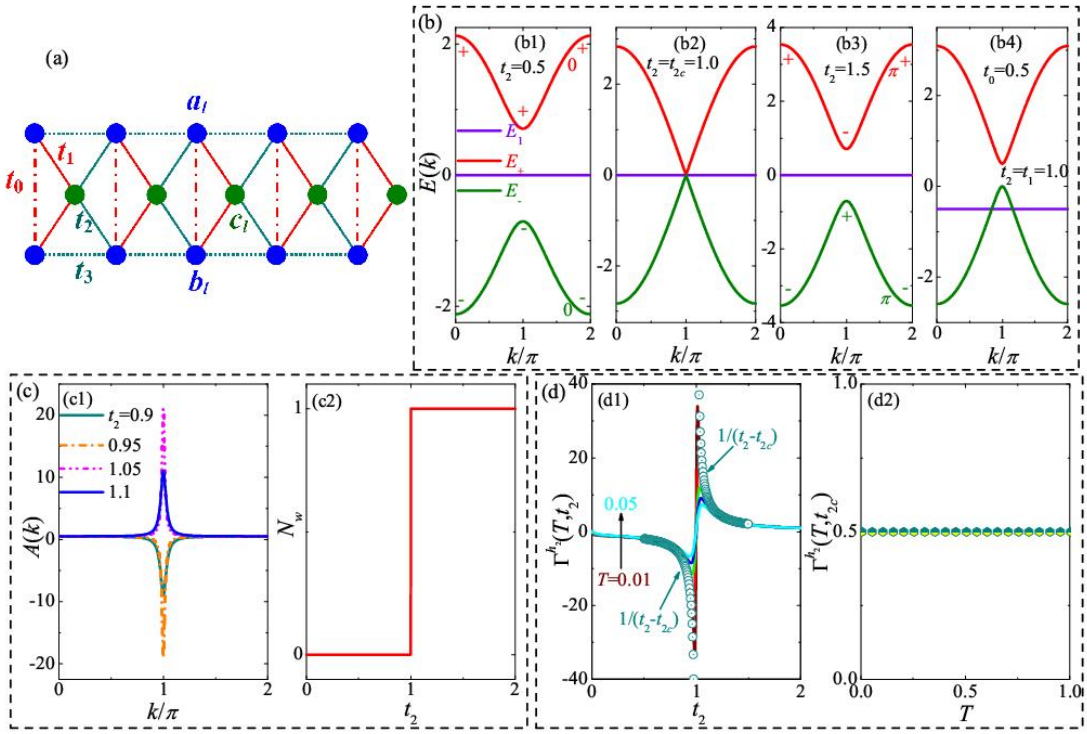

Fig. 1 (a) Schematic of three-leg diamond lattices with each unit cell containing three sublattices (a, b and c). (b) t_3=t_0=0, energy bands for t_2=0.5, 1.0 and 1.5 in (b1)-(b3); (b4) t_3=0, t_0=0.5. For t_3=t_0=0 in subspace h_2, (c) the Berry connection as a function k around t_{2c}=1.0 in (c1), winding number as a function of t_2 in (c2); (d) t_2 dependence of GR under temperatures [0.01,0.05] with interval 0.01 in (d1), the temperature dependence of GR at the QCP in (d2).

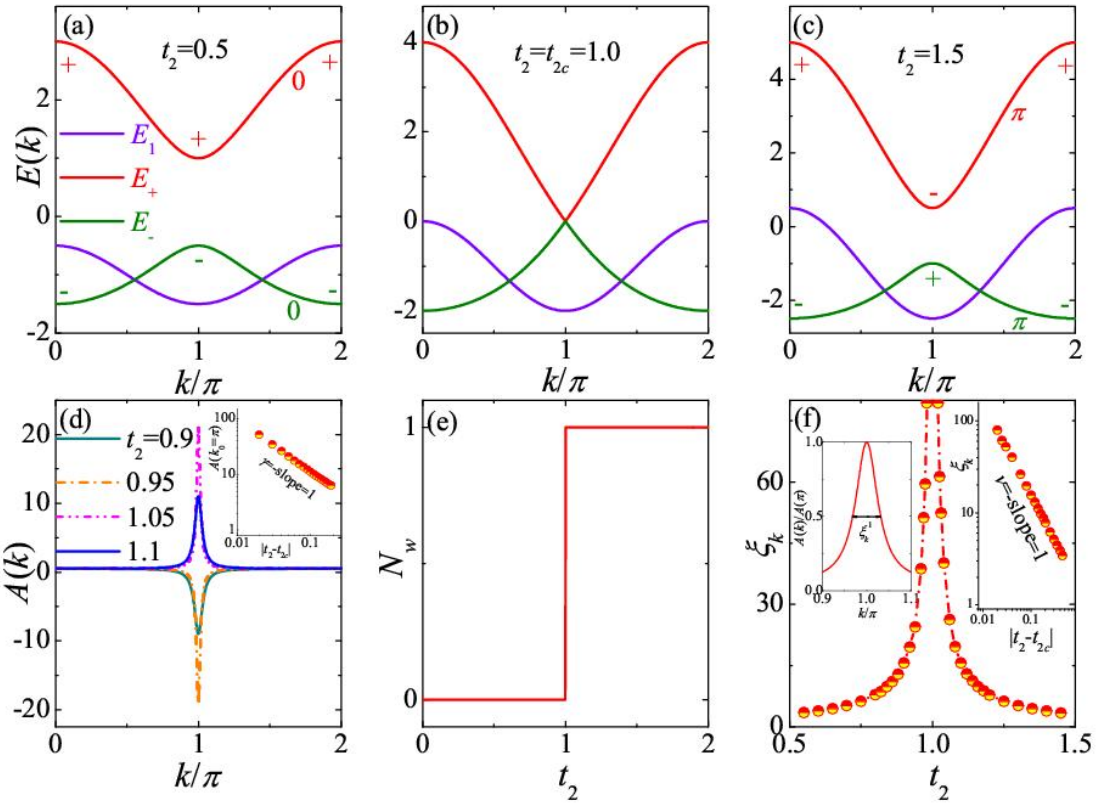

Fig.2 For t_0=t_1, t_3=t_2/2, energy bands for (a) t_2=0.5, (b) t_2=1.0, and (c) t_2=1.5. In subspace h_2,(d) Berry connection as a function k around t_{2c}=1.0; (e) winding number as a function of t_2; (f) t_2 dependence of correlation length, the left inset is the definition of correlation length, while the right inset is its critical scaling.

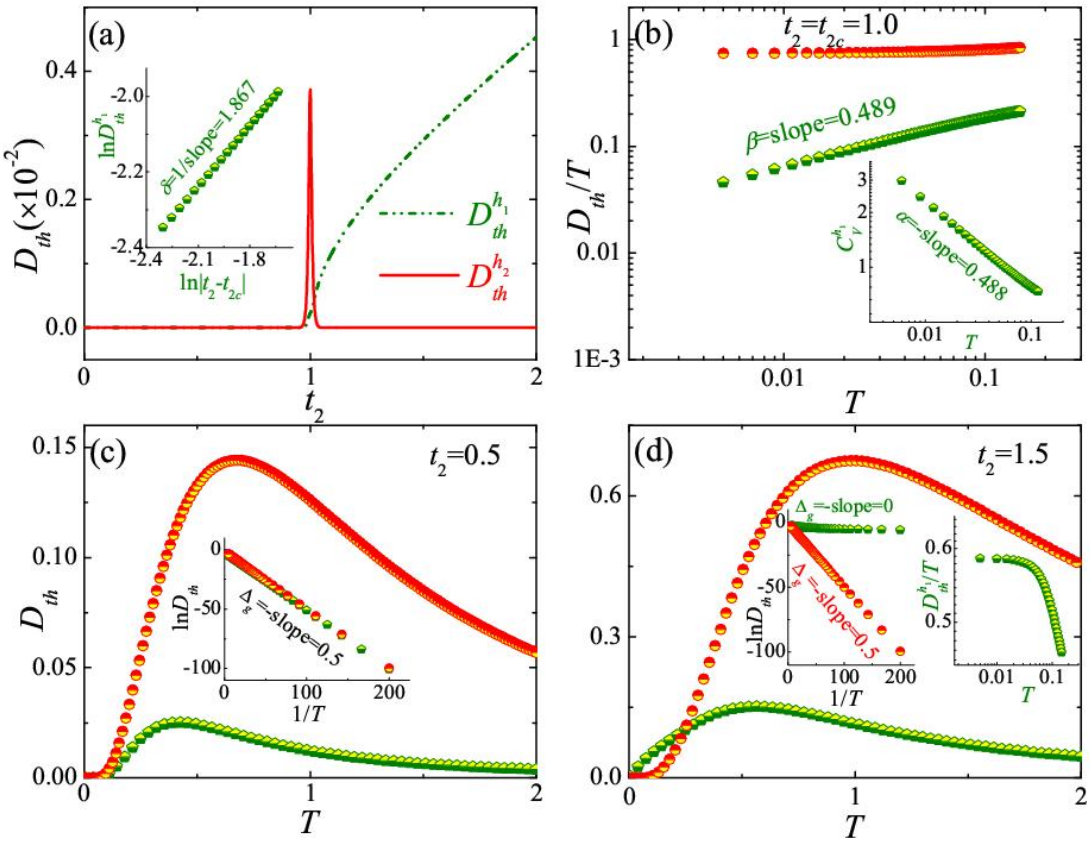

Fig.3 For $t_0=t_1$, $t_3=t_2/2$, (a) t_2 dependence of thermal Drude weight in subspace h_1 (Green) and subspace h_2 (Red), the inset is the critical scaling of thermal Drude weight in h_1 subspace; (b) at the QCP $t_2=t_{2c}=1.0$, $\ln D_{th}/T$ versus lnT in two subspaces, the inset is the critical scaling of specific heat in h_1 subspace; the temperature dependence of thermal Drude weight in two subspaces for (c) $t_2=0.5$, and (d) $t_2=1.5$, the inset in (c) is the curve of $\ln D_{th}$ versus $1/T$, the left inset in (d) is the curve of $\ln D_{th}$ versus $1/T$, while the right inset is the temperature dependence of D_{th}/T in h_1 subspace.

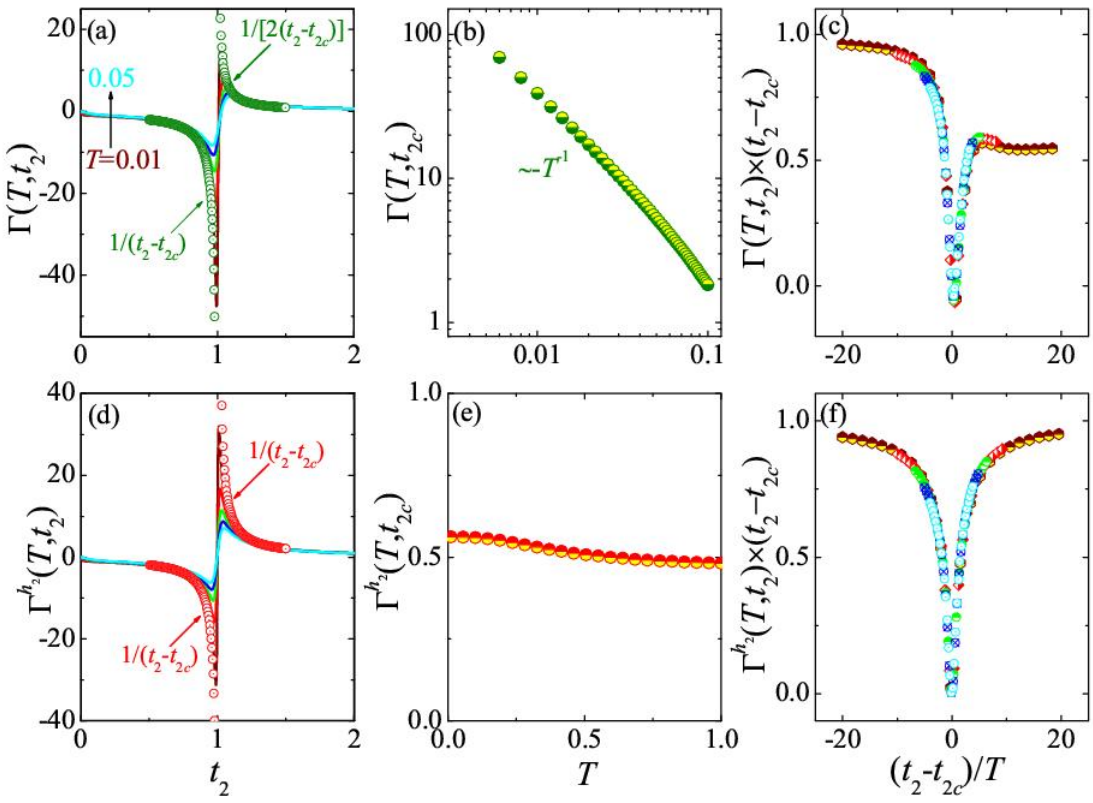

Fig.4 For t_0=t_1, t_3=t_2/2, in whole Hilbert space, (a) t_2 dependence of GR under temperatures [0.01,0.05] with interval 0.01; (b) the temperature dependence of GR at the QCP; (c) the scaling of GR versus rescaled t_2 hopping under different temperatures, all the data points collapse onto an asymmetric universal curve, implying the ordinary insulator-metal transition. In h_2 subspace, (d) GR as a function of t_2 under temperatures [0.01,0.05] with interval 0.01; (e) the temperature dependence of GR at the QCP; (e) the scaling of GR versus rescaled t_2 hopping under different temperatures, all the data points fall onto a symmetric universal curve, indicating the TI transition.